Available online at www.sciencedirect.com

ScienceDirect

Journal of Solid State Chemistry 179 (2006) 3167–3183

JOURNAL OF SOLID STATE CHEMISTRY

www.elsevier.com/locate/jssc

Nonstoichiometry in oxides and its control

Pavel Karen*

Department of Chemistry, University of Oslo, POB 1033 Blindern, N-0315 Oslo, Norway

Received 11 April 2006; received in revised form 24 May 2006; accepted 11 June 2006
Available online 16 June 2006

Abstract

A point–defect scheme is methodically outlined for description of oxygen nonstoichiometry in extended structures of oxides. Two cases of nonstoichiometry are treated; a narrow-range nonstoichiometry centered at an integer valence state of the non-oxygen atom, and a wide-range nonstoichiometry extending between two integer structures. The latter term is introduced as a counterpart to the integer valence (stoichiometry), because for doped oxides these two situations do not coincide on the oxygen partial-pressure scale. The description of the narrow nonstoichiometry is exemplified on a corundum-type oxide (Cr_2O_3; chosen for its nontrivial atom ratio and clear red–ox properties whereas no actual experimental data are treated) and includes the effects of doping. The wide-range nonstoichiometry model is exemplified by $YBa_2Cu_3O_{6+w}$ and tested on experimental data from the literature. Techniques of the oxygen nonstoichiometry control are sorted out according to the controlled variables. Types of analyses of the bulk oxygen nonstoichiometry and of its distribution across the sample are described.

© 2006 Elsevier Inc. All rights reserved.

Keywords: Nonstoichiometry control and analysis; Point defects; Oxides

1. Introduction

Tailoring of properties in functional oxide ceramics depends on effective and precise control of the oxygen nonstoichiometry. This is not only because specific electronic, magnetic and optical properties are coupled to specific valence states of the metal atoms in these oxides, but also because even a small nonstoichiometry may frustrate the desired properties, such as magnetic coupling or valence mixing. In other cases, certain presence of nonstoichiometric defects is desirable, such as in ionic and/or electronic conductors in batteries, fuel cells, gas-separating membranes and chemical sensors. In any case, the property control of a functional oxide begins with a point–defect model of the oxygen content. This is also the starting point of this tutorial, which is followed by chapters on experimental methods of the oxygen-content control and analysis in solid oxides.

1.1. Which oxides are nonstoichiometric?

It has been said on occasion that all oxides, on some level, are nonstoichiometric. However, for molecular oxides, such as CO_2, nonstoichiometry would be equivalent to formation of another oxide molecule, such as CO. To talk about nonstoichiometry only has a meaning for extended-network structures. As we shall see shortly, formation of defects in such networks is based on the entropy principle because the atomic sites in a network are distinguishable, unlike free molecules in a gas. Owing to the individuality of such sites, we talk of *point defects*, as opposed to extended defects, such as dislocations. Whether ionic or covalent, any bond network may become detectably nonstoichiometric under formation of point defects. To name two extreme examples: under ionizing radiation, NaCl becomes colored by formation of a pair of defects, an anion vacancy and an anion interstitial [1]. The ultimately covalent diamond acquires a greenish color [2] upon formation of vacancies and interstitials [3]. However, these radiation-induced defects are not those of thermal equilibrium and disappear upon annealing. Let us limit the scope to those point defects that are formed in thermal

---

*Fax: +47 22 85 54 41.
E-mail address: pavel.karen@kjemi.uio.no.

0022-4596/$ - see front matter © 2006 Elsevier Inc. All rights reserved.
doi:10.1016/j.jssc.2006.06.012

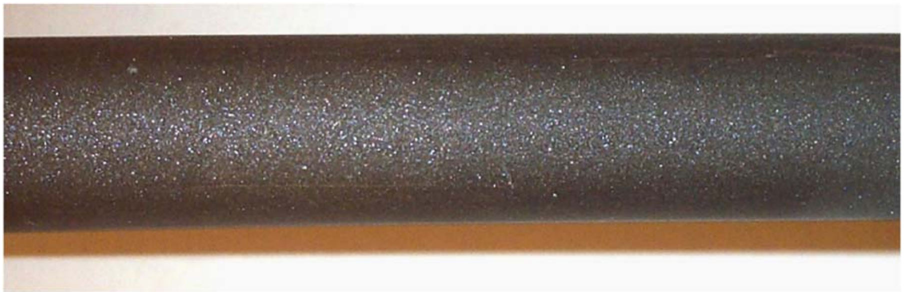

Fig. 1. An originally white corundum rod after exposure to hydrogen at 1400 °C.

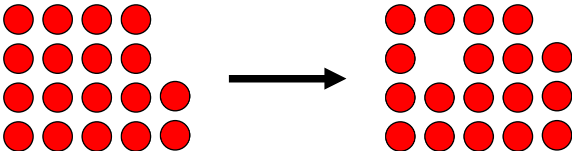

Fig. 2. Vacancy formation in an ideal crystal.

equilibrium and turn back to oxides for the last example of a visible defect formation: when pure sintered corundum, Al_2O_3, is put into hydrogen atmosphere at 1400 °C for several hours, the originally white material becomes shiny black. This black surface layer has composition about $Al_2O_{2.97}$ (Fig. 1).

1.2. Entropy favors defects

Let us consider an ideal crystal in two dimensions, formed by single type of atoms residing at N_0 atomic sites (Fig. 2). A vacancy is created, as though by moving one atom from its regular site to a new site on the outside. The amount of sites becomes N_0+1. What is the Gibbs energy of creating n such isolated, non-interacting, vacancies?

The driving force behind the vacancy creation is the configurational entropy, $kT\ln\Omega$, where Ω is the number of ways n vacancies can be arranged in the N_0+n sites, calculated as permutations $\Omega=(N_0+n)!/(N_0!n!)$. Because $\Delta G=\Delta H-T\Delta S$, the Gibbs energy will have both entropy and enthalpy contributions. For low-vacancy concentrations, two of these contributions will be linear functions of the number of vacancies n: the enthalpy ΔH of the vacancy formation by a net breaking of some bonds and the increase in the vibration entropy ΔS_v associated with the formation of the vacancy. In total, $\Delta G=n(\Delta H-T\Delta S_\mathrm{v})-kT\ln\Omega$ for formation of n vacancies. Fig. 3 shows ΔG as a function of n. It is seen that owing to the nonlinearity of the configurational entropy term, a small equilibrium amount of vacancies n_eq will be formed. This amount corresponds to the minimum in ΔG, which is evaluated by differentiation according to n:

$$\frac{\mathrm{d}}{\mathrm{d}n}\left(n\Delta H-nT\Delta S_\mathrm{v}-kT\ln\frac{(N_0+n)!}{N_0!n!}\right)=0.$$

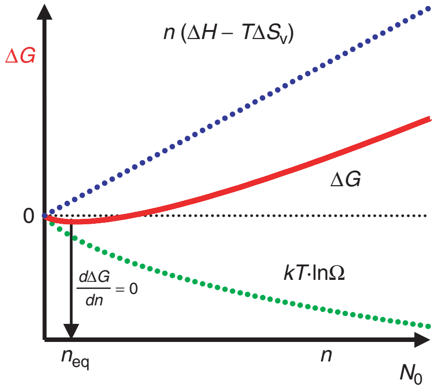

Fig. 3. Gibbs energy of formation of n vacancies in an ideal crystal of N_0 sites.

The factorial term calls for application of the Stirling formula, $\ln(x!)\approx x\ln x-x$ for large x, leading to a profound simplification:

$$\Delta H-T\Delta S_\mathrm{v}-kT\,\ln\left(\frac{N_0+n_\mathrm{eq}}{n_\mathrm{eq}}\right)=0.$$

Note that the term involving n_eq is the inverse of the fractional concentration of the vacancies formed. A rearrangement shows that the fractional concentration of vacancies is a sole function of temperature, with two parameters, ΔH and ΔS_v, occurring in a mass-action-type term:

$$\frac{n_\mathrm{eq}}{N_0+n_\mathrm{eq}}=\exp\left(\frac{\Delta S_\mathrm{v}}{k}-\frac{\Delta H}{kT}\right). \tag{1}$$

This suggests that *equilibrium concentrations*[1] of non-interacting[2] point defects can be treated by the mass-action law.

---

[1] It needs to be emphasized that relatively high temperatures are needed to achieve such equilibria in solid oxides.

[2] If defects interact, defect clusters need to be considered; separately for each section of the nonstoichiometry range where they occur.

1.3. Narrow and wide nonstoichiometry in oxides, integer valence and integer structure

In an extended structure of a metal oxide, thermodynamics will favor formation of small amounts of defects. Their presence will lead to a narrow range of oxygen nonstoichiometry located around the stoichiometric situation that corresponds to the *integer valence* of the metal, or in its immediate vicinity. On the other hand, wide nonstoichiometry would occur between two related, whole, *integer structures* that form a solid-solution range, or between end members of an infinitely adaptive structure [4] series. The term *integer structure* is introduced here as a counterpart to the *integer valence*. An integer structure has the ratio of anions and cations precisely as given by the stoichiometric fraction of the structure's regular sites. It occurs at a point where intrinsic cation and anion defects compensate each other. Both the narrow and wide types of nonstoichiometry will be exemplified in the following.

2. Cr_2O_3 as an example for the narrow nonstoichiometry

Chromium is a typical transition metal with rich red–ox chemistry. This makes the red–ox point defects in its trivalent oxide chemically intuitive. In relation to Fig. 1, it may also be noted that chromium sesquioxide crystallizes with the corundum type. The treatment of the oxygen nonstoichiometry is an attempt to provide a brief methodical description of setting up point–defect equilibria in an oxide, following the classical works of Kröger–Vink [5], Kofstad [6] and, recently, Smyth [7].

2.1. Point defects in pure Cr_2O_3

Formation of both chromium and oxygen vacancies in direct analogy to the entropy example in Fig. 2 is one possible scenario of point defects in this oxide. Such a combination is called a Schottky defect pair. The only difference against the single-atom case is the necessity to maintain the electroneutrality of the compound. The crystal cannot acquire a charge. That means that the metal and oxygen vacancies formed must compensate each other. The electroneutrality balance follows the Kröger–Vink symbolism of point defects [5], in which the *effective charge* of the defect is calculated as a difference from the ideal crystal. In other words, the effective charge of a defect is the real charge of the isolated defect specie minus the real charge of its site in the ideal (defect-free) crystal. The identity of this ideal site is noted in the subscript by the chemical symbol or an "i" if the defect is an interstitial atom. The effective charge appears in the superscript; as a prime for one negative charge, a dot for one positive charge, and a cross for no charge.

Table 1
Possible intrinsic defect processes in Cr_2O_3

Process	Reaction
Schottky	$\mathrm{Nil} = 2v_{\mathrm{Cr}}''' + 3v_{\mathrm{O}}^{\bullet\bullet}$
Anti-Schottky	$2Cr_{\mathrm{Cr}}^{\times} + 3O_{\mathrm{O}}^{\times} = 2Cr_{\mathrm{i}}^{\bullet\bullet\bullet} + 3O_{\mathrm{i}}''$
Cation Frenkel	$Cr_{\mathrm{Cr}}^{\times} = v_{\mathrm{Cr}}''' + Cr_{\mathrm{i}}^{\bullet\bullet\bullet}$
Anion Frenkel	$O_{\mathrm{O}}^{\times} = v_{\mathrm{O}}^{\bullet\bullet} + O_{\mathrm{i}}''$
Intrinsic ionization	$\mathrm{Nil} = e' + h^{\bullet}$

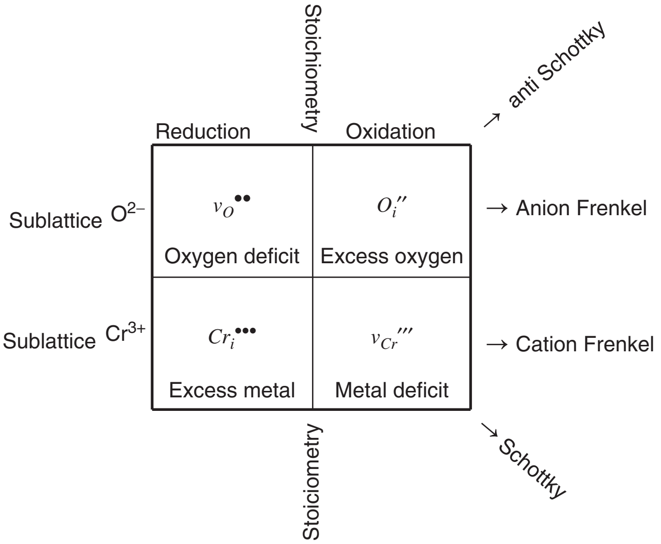

Fig. 4. Possible structural defect compensations for chemical reduction (to the left of the center) and oxidation (to the right) of a pure, stoichiometric Cr_2O_3.

Reactions that describe formation of *intrinsic defects* in a pure and perfectly stoichiometric oxide are listed in Table 1. The term "nil" is to denote that N_0 crystallographic sites are present on both sides of the equation (see also Fig. 2). The first four reactions in Table 1 concern structural defects and one of the equations is a combination of the other three. The last equation concerns electronic defects, and describes thermal excitation of an electron from a valence band to a conduction band, which leaves a hole behind in the valence band. In nonmetallic oxides of transition metals with distinct red–ox behavior, the electron becomes trapped close to the conduction band as the red–ox impurity state Cr^{2+} ($e' \rightarrow Cr_{\mathrm{Cr}}'$) whereas the hole is trapped as a Cr^{4+} state close to the valence band ($h^{\bullet} \rightarrow Cr_{\mathrm{Cr}}^{\bullet}$). Being respectively larger and smaller than the trivalent ions, both defects behave as polarons. It should also be noted that writing full effective charges to vacancies and interstitials in fact is an approximation, not unlike the one behind the solubility product of analytical chemistry. The more correct alternative would be to also consider the ionization of vacancies (when charges become attached to their neighbors) with an additional series of equilibria. For many cases, however, the approximation with the full vacancy/interstitial charge will suffice, just like the solubility product for a poorly soluble salt of a polyprotic acid does. This is because the entire series of ionization reactions tends to occur almost simultaneously.

Table 2
Two compensations of the oxidative nonstoichiometry in Cr_2O_3

	The auxiliary full equations	Equations for oxidation
v_{Cr}'''	$Cr_2O_3 + \delta O = 2/3\delta v_{Cr}''' + 2\delta h^{\bullet} + \delta O_O^{\times} + 2Cr_{Cr}^{\times} + 3O_O^{\times}$	$3O_{2(g)} = 4v_{Cr}''' + 12h^{\bullet} + 6O_O^{\times}$
O_i''	$Cr_2O_3 + \delta O = \delta O_i'' + 2\delta h^{\bullet} + 2Cr_{Cr}^{\times} + 3O_O^{\times}$	$O_{2(g)} = 2O_i'' + 4h^{\bullet}$

Table 3
Two compensations of the reductive nonstoichiometry in Cr_2O_3

	The auxiliary full equations	Equations for reduction
$Cr_i^{\bullet\bullet\bullet}$	$Cr_2O_3 – \delta O = 2/3\ \delta Cr_i^{\bullet\bullet\bullet} – 2/3\ \delta Cr_{Cr}^{\times} + 2\delta e' – \delta O_O^{\times} + 2Cr_{Cr}^{\times} + 3O_O^{\times}$	$4Cr_{Cr}^{\times} + 6O_O^{\times} = 4Cr_i^{\bullet\bullet\bullet} + 12e' + 3O_{2(g)}$
$v_O^{\bullet\bullet}$	$Cr_2O_3 – \delta O = \delta v_O^{\bullet\bullet} + 2\delta e' – \delta O_O^{\times} + 2Cr_{Cr}^{\times} + 3O_O^{\times}$	$2O_O^{\times} = 2v_O^{\bullet\bullet} + 4e' + O_{2(g)}$

2.2. *Reducing and oxidizing the pure oxide; red–ox compensations*

The possible responses of intrinsic defects in Cr_2O_3 to chemical oxidation and reduction are outlined in Fig. 4. When the precisely stoichiometric Cr_2O_3 is reduced, a deficit of oxygen or an excess of metal can be created. Upon oxidation, either an excess of oxygen, or a deficit of metal may be the response of the structure. Fig. 4 shows that these alternative responses are based on the four possible intrinsic point-defect reactions listed in Table 1. Which of them actually dominates in the real oxide is a question that needs tedious studies to be answered. Often, no firm conclusions can be reached [8].

2.3. *Defect-equilibrium equations for oxidative and reductive nonstoichiometry in Cr_2O_3*

Independent of the actual red–ox compensation, oxidation of the oxide shall mean here a reaction with O_2 from the reaction atmosphere.[3] This reaction needs to be balanced so that it is apparent which species are in equilibrium when the solid oxide is in contact with O_2 at high temperatures. The balancing may follow a simple scheme (Table 2) starting with 1 mol of Cr_2O_3 and δ oxygen atoms, which is then simplified by crossing out species occurring at both sides, changing to $O_{2(g)}$ and removal of fractions. The reductive nonstoichiometry is treated analogously in Table 3 as a process of the removal of the oxygen atoms from the oxide. So far, the treatment has been general, but at this point one needs to select the actual pair of equations from Table 3 and Table 4 for one of the four red–ox-compensating point-defect combinations in Fig. 4.

Table 4
Schottky-type red–ox compensation in Cr_2O_3

Process	Reaction	Mass-action term[a]
Schottky	$\mathrm{Nil} = 2v_{Cr}''' + 3v_O^{\bullet\bullet}$	$K_S = [v_{Cr}''']^2[v_O^{\bullet\bullet}]^3$
Ionization	$\mathrm{Nil} = e' + h^{\bullet}$	$K_i = [e'][h^{\bullet}]$
Oxidation	$3O_{2(g)} = 12h^{\bullet} + 4v_{Cr}''' + 6O_O^{\times}$	$[v_{Cr}''']^4[h^{\bullet}]^{12} = K_{ox} \cdot p_{O_2}^3$
Reduction	$2O_O^{\times} = 4e' + 2v_O^{\bullet\bullet} + O_{2(g)}$	$[v_O^{\bullet\bullet}]^2[e']^4 = K_{red} \cdot p_{O_2}^{-1}$

[a] The oxygen pressure p_{O_2} is in units of the standard state P° to be specified when numerical data are reported.

2.4. *Defect equilibria for Schottky-type red–ox compensation*

For the Cr_2O_3 model case, we shall in the following assume that the dominant defects are of the Schottky type.[4] There will be two intrinsic reactions and two chemical reactions, one for oxidation and one for reduction. Their equilibria are summarized in Table 4.

Only three of these four equations are independent, as we can see from evaluating that $K_S \cdot K_i^6 = K_{ox} \cdot K_{red}^3$. A fourth equation is needed, because there are four unknown concentrations: of holes, electrons, chromium and oxygen vacancies. This fourth equation is provided by the electroneutrality condition: $3[v_{Cr}'''] + [e'] = [h^{\bullet}] + 2[v_O^{\bullet\bullet}]$.

The four equations chosen can be rearranged so that each of them contains concentration of only one type of defect as a function of the partial pressure of oxygen p_{O_2}, with three equilibrium constants as parameters. Such equations are polynomials of higher order and the defect concentrations need to be solved numerically. Once this is done, the oxygen nonstoichiometry can be evaluated as a function of p_{O_2}. Because the defect concentrations refer to the unit of structure sites, it may be convenient to maintain the sum of the regular site fractions and express the nonstoichiometry w as *per pseudoatom*, $Cr_{2/5}O_{3/5+w}$. Therefore, $w = (3/2)[v_{Cr}'''] – [v_O^{\bullet\bullet}]$.

---

[3] Oxidations with O_3 or oxygen plasma would be treated analogously. Participation of chromium vapor is not considered and would require two more red–ox equations of which one would be independent.

[4] As in the structural prototype, corundum.

In Fig. 5, the defect concentrations and the oxygen excess w are plotted as a function of p_{O_2} for the hypothetical case that the Schottky defects (and not electronic defects) dominate in the pure stoichiometric oxide. We can identify the point of the integer valence, which is the stoichiometric situation when the electronic defects compensate each other, $[e'] = [h^\bullet]$, and we see the point of the integer structure where the intrinsic structural defects compensate each other, $3[v_{Cr}'''] = 2[v_O^{\bullet\bullet}]$. In the pure oxide, these two points coincide on the p_{O_2} scale.

There are three significant situations where the dependences on p_{O_2} are becoming linear with specified fractional slopes. In the middle region, the Schottky vacancies dominate. In the most oxidized region, holes are compensated predominantly by metal vacancies. In the most reduced region, electrons are compensated predominantly by oxygen vacancies. When the electroneutrality condition is limited to these dominant defects for each region, linear dependences are obtained. As an example, the electroneutrality condition for the oxidized region becomes simply $3[v_{Cr}'''] = [h^\bullet]$, and a substitution from here for $[h^\bullet]$ into the mass-action term in the fourth row of Table 4 shows that $[v_{Cr}''']$ is proportional to $p_{O_2}^{3/16}$.

A change in equilibrium constants of the defect reactions may completely alter the picture of the defect concentrations around the integer-valence point ($[e'] = [h^\bullet]$). Yet, as seen in Fig. 6, the curve for the oxygen nonstoichiometry w is very similar to the previous case in Fig. 5. This is because w is detectably changing only in the most oxidized and most reduced regions where the limiting slopes for the vacancy concentrations remain unchanged. It is clear that the difference in defect concentrations around the stoichiometric point is not to be decided from the oxygen nonstoichiometry measurements, or these alone, but rather from data on electronic conductivity. Such data for Cr_2O_3, for example, in Ref. [9], suggest that electronic defects dominate in this range over the structural defects.

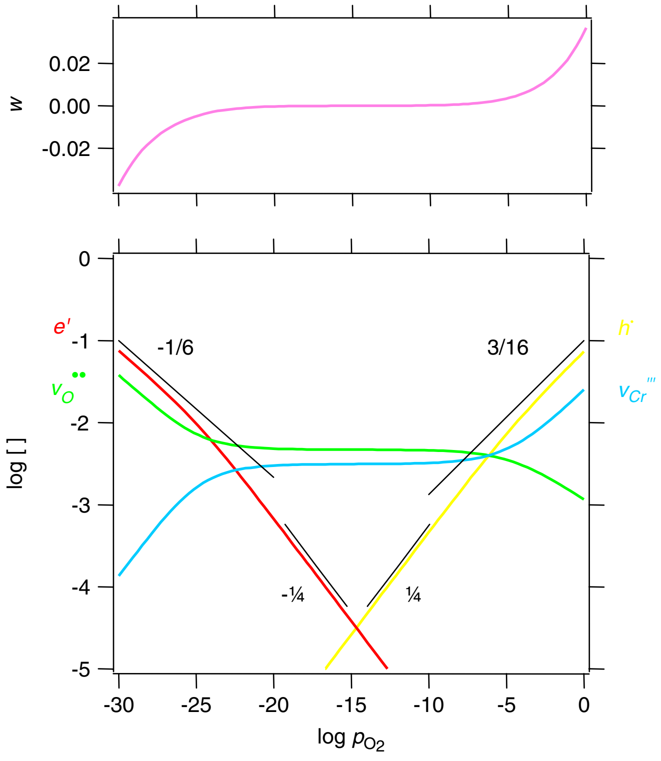

Fig. 5. Defect concentrations in hypothetical chromium sesquioxide with dominant Schottky defects ($K_i = 10^{-9}$, $K_{ox} = 10^{-10}$, $K_S = 10^{-12}$). The oxygen nonstoichiometry $w = (3/2)[v_{Cr}''']-[v_O^{\bullet\bullet}]$ refers to the pseudoatom formula $Cr_{2/5}O_{3/5+w}$.

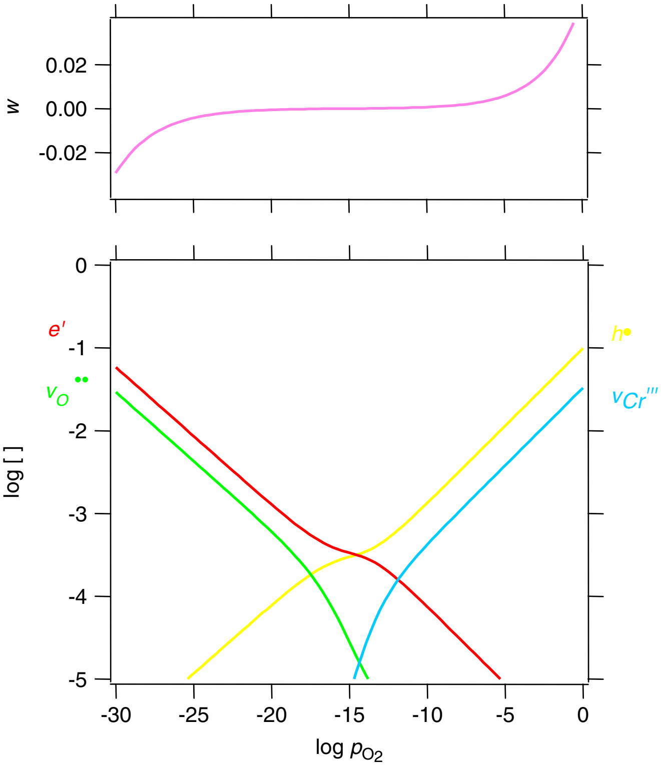

Fig. 6. Defect concentrations in hypothetical chromium sesquioxide with Schottky and electronic defects in comparable concentrations ($K_i = 10^{-7}$, $K_{ox} = 10^{-9}$, $K_S = 10^{-24}$). The oxygen nonstoichiometry $w = (3/2)[v_{Cr}''']-[v_O^{\bullet\bullet}]$ refers to the pseudoatom formula $Cr_{2/5}O_{3/5+w}$.

2.5. *Acceptor-doped oxide*

Let us replace a small[5] portion of Cr^{3+} with a divalent ion of irrelevant red–ox properties, for example, Mg^{2+}. The pseudoatom formula is then $Cr_{2/5-x}Mg_xO_{3/5+w}$. All equations from Table 4 for the pure oxide remain the same. The only difference appears in the electroneutrality equation which now includes the extrinsic defect: $3[v_{Cr}'''] + [e'] + [Mg_{Cr}'] = [h^\bullet] + 2[v_O^{\bullet\bullet}]$.

The derivation of the equations for defect concentrations as functions of the partial pressure of oxygen is very much analogous to that for the pure oxide, except that there are now four parameters controlling the defect equilibria: the three equilibrium constants and the concentration of the acceptor defect $[Mg_{Cr}'] = x$.

---

[5] The acceptor solubility is generally not independent of the partial pressure of oxygen, but let us assume that the doping level x is less than the solubility of the acceptor for all considered p_{O_2}.

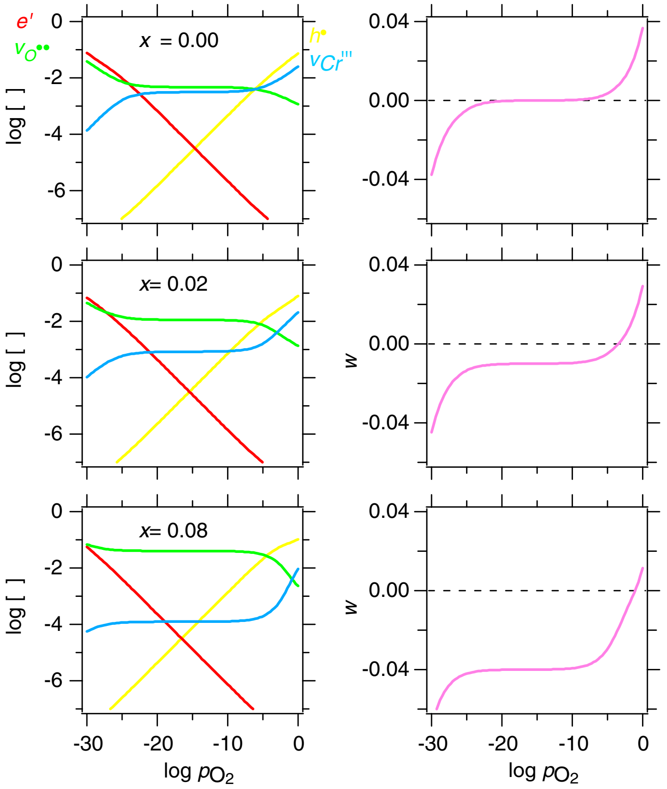

Fig. 7. Acceptor doping by magnesium. Defect concentrations in hypothetical chromium sesquioxide with predominant Schottky defects ($K_i = 10^{-9}$, $K_{ox} = 10^{-10}$, $K_S = 10^{-12}$) for several levels x of acceptor doping. The oxygen nonstoichiometry $w = (3/2)[v_{\mathrm{Cr}}''']-[v_{\mathrm{O}}^{\bullet\bullet}]$ refers to the pseudoatom formula $\mathrm{Cr}_{2/5-x}\mathrm{Mg}_x\mathrm{O}_{3/5+w}$.

While the acceptor defect does not affect much the process of solving the equations, it changes profoundly the result. In Fig. 7, the defect concentrations and the corresponding oxygen nonstoichiometry w are plotted for x increasing from zero. With increasing x, the point of integer valence ($[e'] = [h^{\bullet}]$) moves to the left, the point of integer structure ($3[v_{\mathrm{Cr}}'''] = 2[v_{\mathrm{O}}^{\bullet\bullet}]$) moves to the right. The former shift, toward low p_{O_2}, means that trivalent chromium is oxidized more easily than in the pure oxide. The latter shift, toward higher p_{O_2}, means that oxygen vacancies in the integer structure are created more easily. Both statements concern only the portion of holes $h^{\bullet}$ or oxygen vacancies $v_{\mathrm{O}}^{\bullet\bullet}$ that is equivalent to the Mg acceptor.

Note that Fig. 7 shows the case when K_S is high, that is, when Schottky defects prevail over the electronic defects. One dominant plateau in the oxygen-nonstoichiometry w occurs, situated above the point of integer valence ($[e'] = [h^{\bullet}]$). At this plateau, the acceptor is compensated by oxygen vacancies and practically not by holes because their concentration is too low. Varied level of the acceptor doping affects the w dependence mainly by shifting it vertically. This picture changes profoundly when neither structural nor electronic defects prevail (Fig. 8).

Already a low level of acceptor doping ($x = 0.001$) brings about significant departures of the points of integer valence ($[e'] = [h^{\bullet}]$) and integer structure ($3[v_{\mathrm{Cr}}'''] = 2[v_{\mathrm{O}}^{\bullet\bullet}]$) from each other. At this moment the effect on w is very small, but upon increasing acceptor doping two distinct w plateaus are formed on the plot versus p_{O_2}. One occurs at low oxygen pressures, when the acceptor is compensated by oxygen vacancies, and is centered on the point of integer valence. The other occurs at higher oxygen pressures, when the acceptor is compensated by holes, and is centered on the point of integer structure.

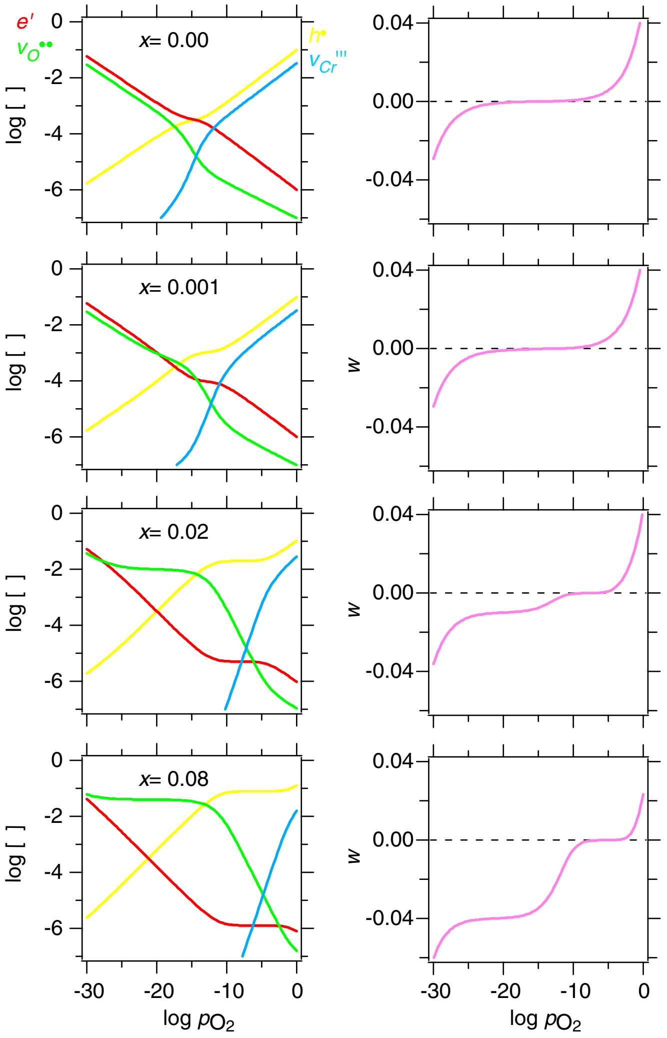

Fig. 8. Acceptor doping by magnesium. Defect concentrations in hypothetical chromium sesquioxide when neither electronic nor Schottky defects prevail ($K_i = 10^{-7}$, $K_{ox} = 10^{-9}$, $K_S = 10^{-24}$) for several levels x of acceptor doping. The oxygen nonstoichiometry $w = (3/2)[v_{\mathrm{Cr}}''']-[v_{\mathrm{O}}^{\bullet\bullet}]$ refers to the pseudoatom formula $\mathrm{Cr}_{2/5-x}\mathrm{Mg}_x\mathrm{O}_{3/5+w}$.

A third distinct case (Fig. 9) is when the concentrations of the structural defects are so low that the oxygen-nonstoichiometry plateau above the point of integer valence practically disappears and only the w plateau above the integer structure point remains. This represents a situation when the acceptor doping $[Mg_{\mathrm{Cr}}'] = x$ is compensated mainly by holes because of the low concentration of oxygen vacancies. It is also close to the real situation in $\mathrm{Cr_2O_3}$, in which the range of constant hole concentration at

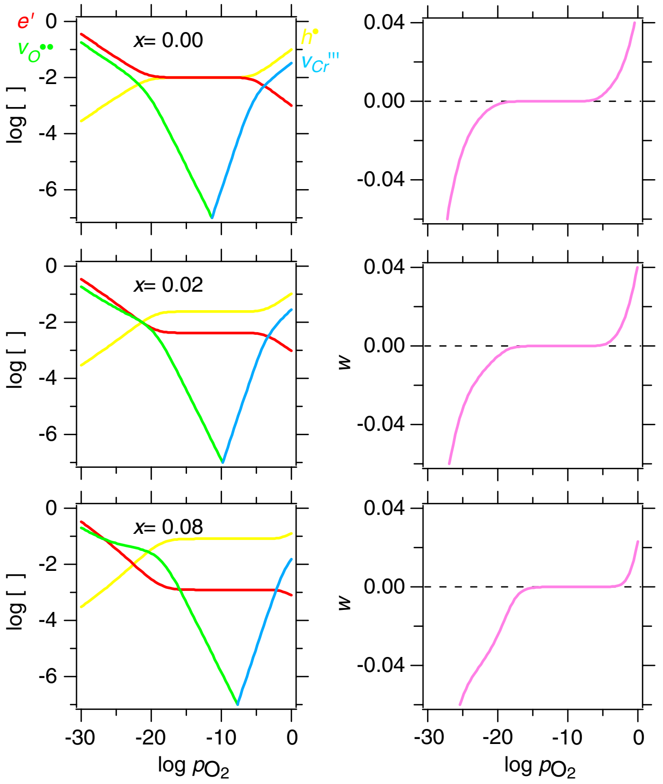

Fig. 9. Acceptor doping by magnesium. Defect concentrations in hypothetical chromium sesquioxide with predominant electronic defects ($K_i = 10^{-4}$, $K_{ox} = 10^{-9}$, $K_S = 10^{-35}$) for several levels x of acceptor doping. The oxygen nonstoichiometry $w = (3/2)[v_{Cr}''']-[v_O^{\bullet\bullet}]$ refers to the pseudoatom formula $Cr_{2/5-x}Mg_xO_{3/5+w}$.

high temperatures extends well over the ambient pressure already for $x = 0.02$ [10].

2.6. Donor-doped oxide

A realistic candidate for donor doping[6] of chromium sesquioxide is $Cr_{2/5-x}Ti_xO_{3/5+w}$. Fig. 10 shows defect concentrations and oxygen nonstoichiometry as a function of the partial pressure of oxygen for case of structural defects (Schottky) prevailing over electronic defects. The situation is the inverse of the acceptor case in Fig. 7: The point of the integer valence ($[e'] = [h^\bullet]$) has moved to the right, toward higher p_{O_2}, and chromium became more easily reducible. The point of integer structure ($3[v_{Cr}'''] = 2[v_O^{\bullet\bullet}]$) has moved to the left, and it is now easier to create chromium vacancies. The oxygen nonstoichomery function mainly moves on the vertical scale showing one distinct plateau when the titanium donor $[Ti_{Cr}^\bullet] = x$ is compensated by chromium vacancies.

In analogy with the acceptor doping (Fig. 8), a different picture appears when neither electronic nor structural defects dominate (Fig. 11). The third case, when electronic

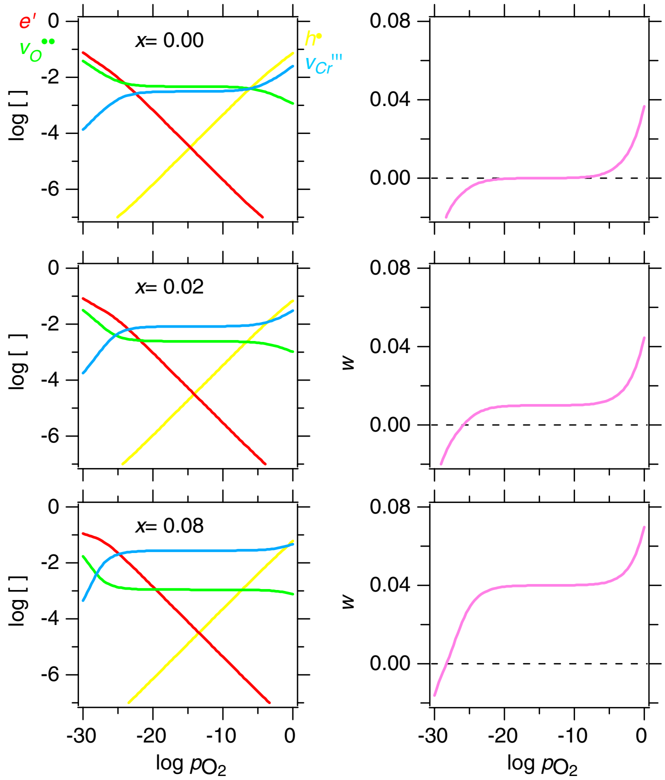

Fig. 10. Donor doping by titanium. Defect concentrations in hypothetical chromium sesquioxide with predominant Schottky defects ($K_i = 10^{-9}$, $K_{ox} = 10^{-10}$, $K_S = 10^{-12}$) for various levels x of donor doping. The oxygen nonstoichiometry $w = (3/2)[v_{Cr}''']-[v_O^{\bullet\bullet}]$ refers to the pseudoatom formula $Cr_{2/5-x}Ti_xO_{3/5+w}$.

defects dominate, is not shown, because it again is a mirror image of the low K_S plots for the acceptor in Fig. 9.

2.7. Note on defects in pure oxides

The idealized defect model for pure hypothetical Cr_2O_3 was one of four equivalent choices (of the four red–ox compensations). It would be further subdivided into differing defect schemes, depending on prevalence in concentration of either structural or electronic defects. Yet the largest caveat of defect modeling in undoped (pure) oxides is that they actually never are undoped. Any oxide has impurities that affect the defect equilibria at some level. But this is not all. While in three-dimensional metallate networks (as in non-vacant perovskites) point defects interact little, some deceptively simple oxides (such as the rock-salt-type wüstite of ideal composition FeO) are grossly nonstoichiometric and the defects are clustered. There is a smooth transition between the nearly ideal situation with diluted and statistically distributed point defects as seen in Cu_2O, NiO, ZnO, Cr_2O_3 (to name only binary oxides) to a quasi-random distribution (CoO), to defect clustering (FeO), to formation of several defect-ordered superstructures (CeO_2, PrO_2) and infinitely adaptive series of defect-ordered structures of crystallographic shear (Magnéli phases as an example) [11]. Even in oxides

---

[6] The donor solubility is generally not independent of the partial pressure of oxygen, but let us assume that the doping level x is less than the solubility of the donor for all considered p_{O_2}.

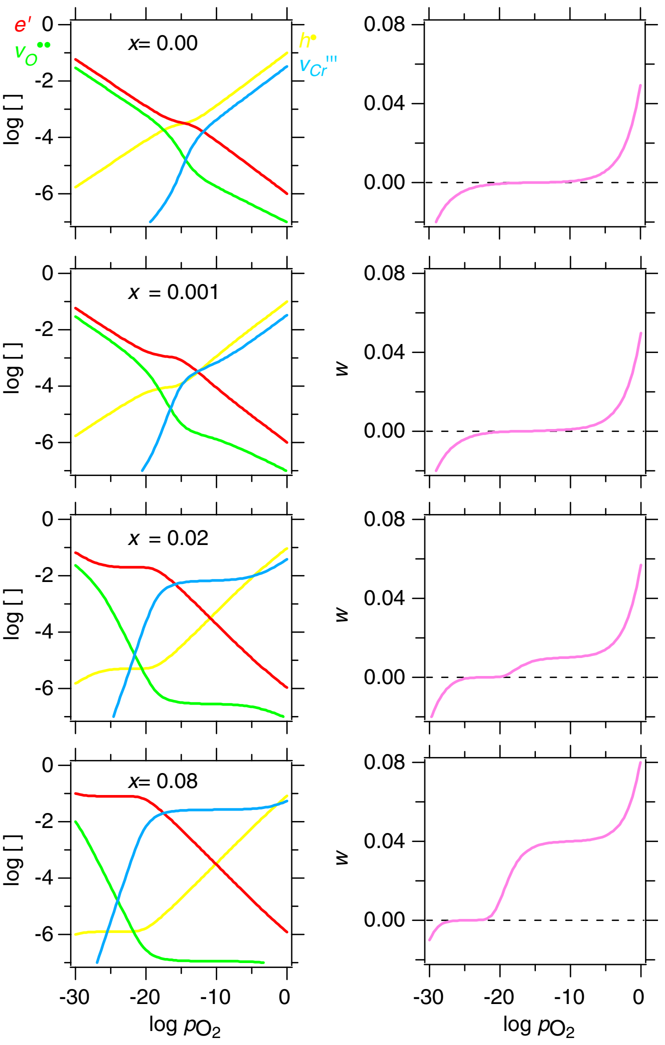

Fig. 11. Donor doping by titanium. Defect concentrations in hypothetical chromium sesquioxide when neither electronic nor structural defects prevail ($K_i = 10^{-7}$, $K_{ox} = 10^{-9}$, $K_S = 10^{-24}$) for various levels x of donor doping. The oxygen-nonstoichiometry $w = (3/2)[v_{Cr}''']-[v_O^{\bullet\bullet}]$ refers to the pseudoatom formula $Cr_{2/5-x}Ti_xO_{3/5+w}$.

with noninteracting defects, clustering may concern dopants (impurities), such as dimerizations or donor–vacancy associations. On the other hand, some complex oxides exhibit rather simple defect equilibria even on the wide nonstoichiometry scale. The next case is one of those.

3. Oxides with wide nonstoichiometry ranges: $YBa_2Cu_3O_{6+w}$

The well-known superconducting cuprate is a typical example of a structure with a wide oxygen-nonstoichiometry range. One entire oxygen atom per formula can be put in or taken out, making the two end members chemically very different phases. Only if the oxygen content is maintained constant (as in Fig. 12), the van't Hoff plot of log(p_{O_2}) versus $1/T$ is linear [12], just like it would be for any chemical reaction that involves a gas.

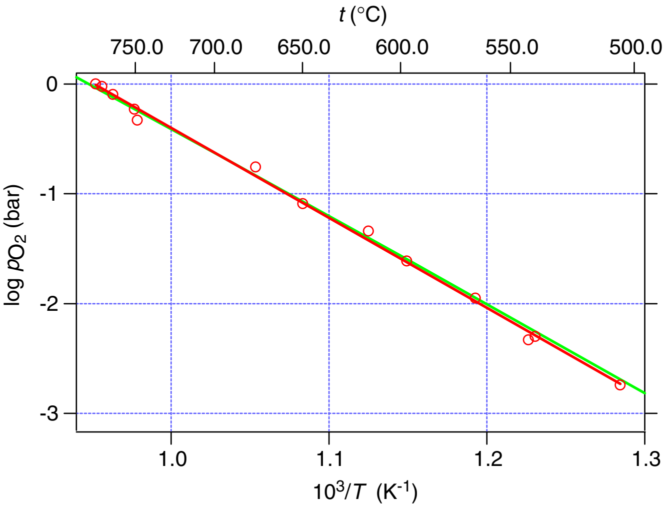

Fig. 12. Equilibrium partial pressure of oxygen versus temperature for constant composition $YBa_2Cu_3O_{6.50}$ (red line and circles), compared with reaction $2BaO_2 \rightarrow 2BaO + O_2$ (green line).

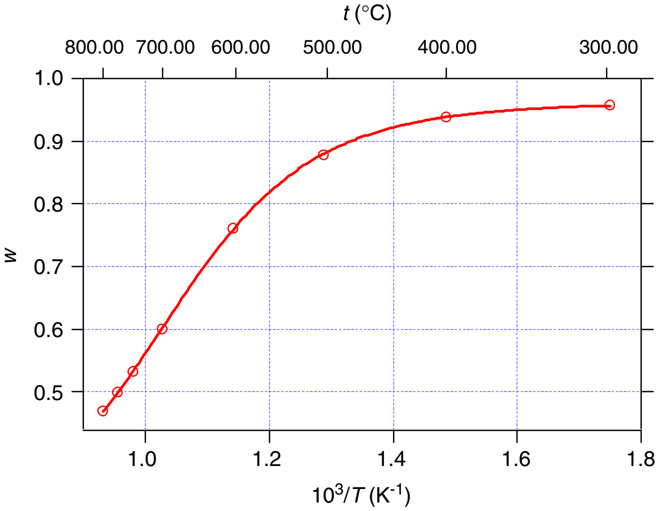

Fig. 13. Oxygen nonstoichiometry in $YBa_2Cu_3O_{6+w}$ as a function of temperature for equilibrium in 1 bar O_2 atmosphere.

A problem is that for $YBa_2Cu_3O_{6+w}$ ($0.00<w<1.00$) we need one line for every w.

As many have experienced, the oxygen content in this phase depends on the temperature regime and the partial pressure of oxygen under the synthesis. This is illustrated by the w, T plot [12] in Fig. 13, from which one very important observation is to be made: there is no plateau at the composition $w = 0.5$ that formally corresponds to the divalent copper. The conclusion is that this average divalent copper does not represent a point of integer valence (stoichiometry) for this phase. Indeed, the more complete data, shown later, will illustrate even better that the oxygen content changes smoothly between $w = 0$ and 1.

In general, two approaches have been used in the literature to describe the oxygen nonstoichiometry in

$YBa_2Cu_3O_{6+w}$: (a) defect models that assume defect clustering, (b) thermodynamic approach of the so-called lattice-gas model. An example of the defect-clustering models is in a study by Maier and Tuller [13] that observes the good linearity of the experimental oxygen-nonstoichiometry isotherms when plotted as $\log[w/(1–w)]$ versus $\log(p_{O_2})$ and utilizes defect clusters to set up the corresponding defect equilibria. In contrast, the lattice-gas model evaluates the partial molar free energy for incorporation of O_2 from standard and excess values of mixing enthalpies and entropies. Examples of the latter approach are Refs. [14,15]. The lattice-gas model has been developed to a rather high degree of complexity as well as precision in Ref. [16]. A more detailed discussion of these methods may be found in Ref. [17]. The treatment shown in the following is not akin to these approaches. In analogy to the treatment of the narrow type of nonstoichiometry, it uses a formal doping of the stoichiometric point to define the oxygen-content range between the two limiting structural situations.

3.1. *The two limiting integer structures for $YBa_2Cu_3O_{6+w}$*

Oxygen nonstoichiometry in $YBa_2Cu_3O_{6+w}$ extends between two structures shown in Fig. 14. In the oxygen-depleted form, one of the two crystallographically different Cu atoms adopts the linear coordination typical of monovalent copper. The other Cu atom must be divalent by virtue of the charge balance. In the oxygen-saturated form, the coordination about the originally monovalent Cu becomes square planar. However, the copper valence in $YBa_2Cu_3O_7$ is clearly not an integer number.

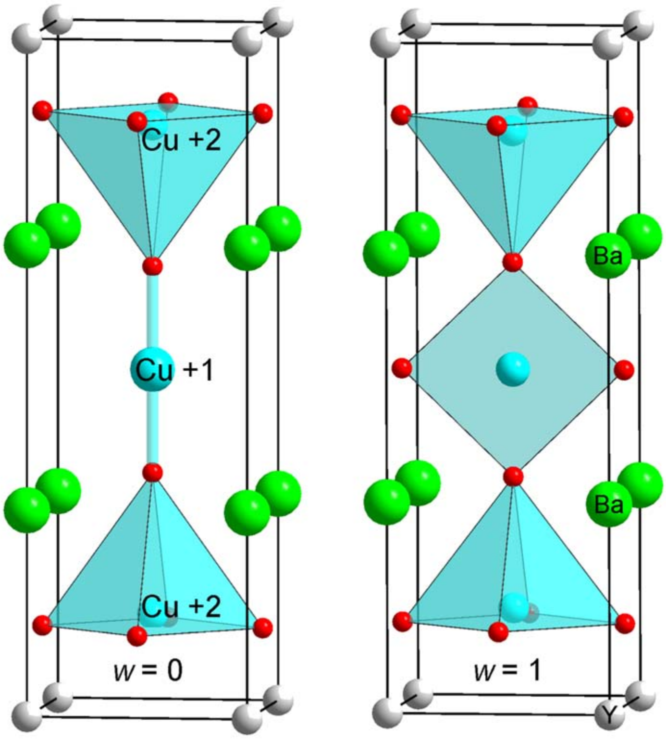

Fig. 14. The two limiting integer structures of $YBa_2Cu_3O_{6+w}$ with copper valences at the point of integer stoichiometry marked in.

3.2. *Where is the point of integer valence for $YBa_2Cu_3O_{6+w}$?*

The point of integer valence appears at the stoichiometric composition that corresponds to the intrinsic situation $[e'] = [h^\bullet]$. The *n* to *p* semiconducting transition occurring at this point is manifested, among other, by a switch in the thermopower sign and occurring minimum in oxygen diffusivity. Of the two integer structures, only the combination of the mono- and divalent copper in $YBa_2Cu_3O_6$ fulfils these criteria [18,19]. Unfortunately, the experimental data are limited by the phase-stability boundary coinciding with this composition. In fact, the ideally stoichiometric phase has never been reached to a reliable degree of precision.

The oxygen-content span between these two integer structures is identical with the extent to which the reduced form is easily oxidized; for example, in contact with O_2. Such an easy-oxidation behavior of a vacant structure is associated with acceptor doping; in this case, a doping by two valence units per formula must be considered. This can formally be achieved by a choice of $Y_3Cu_3O_7$ as the (hypothetical) stoichiometric parent phase, and $2Ba_Y'$ per formula as the dopant [20]. Both red–ox and structural properties are modeled in this manner because this acceptor can either be compensated by one oxygen vacancy per formula giving $YBa_2Cu_3O_6$, or by two electron holes giving $YBa_2Cu_3O_7$. Note that the hypothetical parent phase possesses the integer structure of the oxidized form, whereas it has the integer valences of the reduced form. However, the sole purpose of this formal (integer) doping is to define the other limiting (in this case integer) structure for this phase of wide nonstoichiometry, so that defect equilibria can be set up.

3.3. *The defect equilibria*

The point–defect pair that prevails in the integer structure, be it a Schottky pair, Frenkel pair, etc., is assumed to remain the same irrespective of doping. Because in $YBa_2Cu_3O_{6+w}$ the structural defects of our interest concern the oxygen sublattice, we chose the anion Frenkel combination for the red–ox structural compensation. Accordingly, there will be two intrinsic reactions: the

Table 5
Frenkel-type red–ox compensation in hypothetical pure phase $Y_3Cu_3O_7$

Process	Reaction	Mass-action term[a]
Frenkel	$O_O^\times = v_O^{\bullet\bullet} + O_i''$	$K_F = [v_O^{\bullet\bullet}][O_i'']$
Ionization	$\mathrm{Nil} = e' + h^\bullet$	$K_i = [e'][h^\bullet]$
Oxidation	$\frac{1}{2}O_{2(g)} = 2h^\bullet + O_i''$	$[O_i'][h^\bullet]^2 = K_{ox} \cdot p_{O_2}^{1/2}$
Reduction	$O_O^\times = 2e' + v_O^{\bullet\bullet} + \frac{1}{2}O_{2(g)}$	$[v_O^{\bullet\bullet}][e']^2 = K_{red} \cdot p_{O_2}^{-1/2}$

[a] The pressure refers to the standard state $P^\circ = 1\,\mathrm{bar}$.

Frenkel-defect formation and the intrinsic ionization, and two chemical reactions: one for oxidation and one for reduction. These equilibria are summarized in Table 5.

Three of these four equations with four unknowns are independent ($K_F \cdot K_i^2 = K_{ox} \cdot K_{red}$). The fourth independent equation, to be supplied, is the electroneutrality condition. For the special case of $Y_3Cu_3O_7$ doped with $2Ba_Y'$, the electroneutrality condition expressed per formula is: $2+2[O_i''] + [e'] = [h^\bullet] + 2[v_O^{\bullet\bullet}]$. Each of the four defect concentrations is a polynomial function of the partial pressure of oxygen and can be solved numerically with the three equilibrium constants as parameters.

3.4. Fitting the model to experimental data

The $YBa_2Cu_3O_{6+w}$ oxygen nonstoichiometry is $w = 1-[v_O^{\bullet\bullet}]+[O_i'']$, and the experimental isothermal $w(p_{O_2})$ data can be fitted with this formula by least squares, with three equilibrium constants as parameters. Because $K = \exp((\Delta S^\circ/R) - (\Delta H^\circ/RT))$, also an entire set of $w(p_{O_2}, T)$ data can be fitted, with altogether six parameters. These parameters are the entropy and enthalpy changes for each of those three equilibrium reactions that were chosen to model the oxygen nonstoichiometry. Under the least-squares fitting of the extensive data for $YBa_2Cu_3O_{6+w}$ from the literature [14,15,21,22], it turned out that two of the three entropy parameters were correlating with other parameters while approaching rather small values. For best fit, these two parameters, ΔS°_{ox} and ΔS°_i, were fixed to zero, whereas ΔS°_F was released. The isotherms based on the fitted parameters are plotted in Fig. 15.

An overall glimpse of the raw oxygen-nonstoichiometry data for $YBa_2Cu_3O_{6+w}$ used in the fits is shown in three-dimensional plots in Fig. 16 as a function of the partial pressure of oxygen and reciprocal temperature. The plot on the left-hand side of Fig. 16 shows how the nonstoichio-

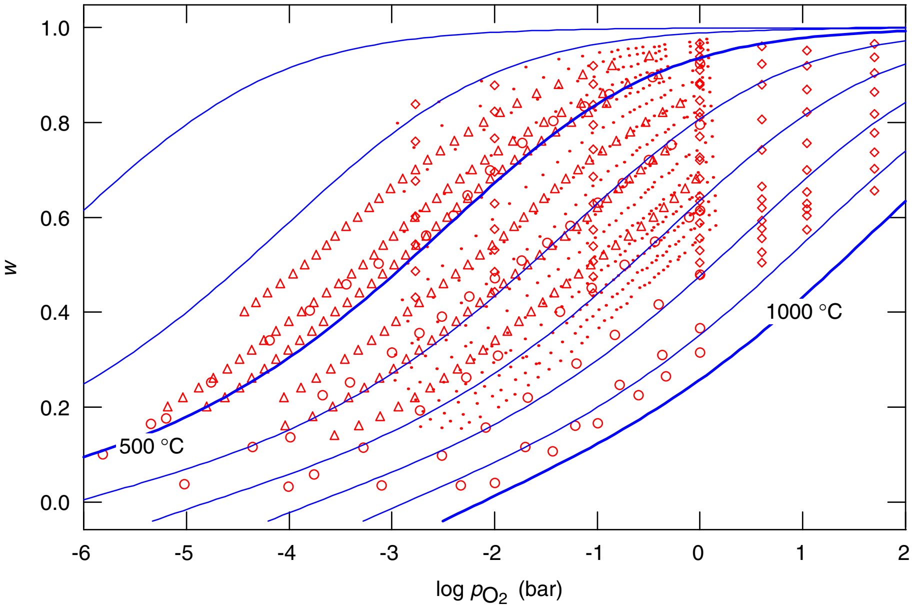

Fig. 15. Oxygen nonstoichiometry in $YBa_2Cu_3O_{6+w}$ as a function of partial pressure of oxygen and temperature: experimental data (dots [14], triangles [15], circles [21], diamonds [22]) and isotherms plotted from the least-squares fitted entropies and enthalpies of defect reactions with equilibrium constants K_i, K_F and K_{ox}.

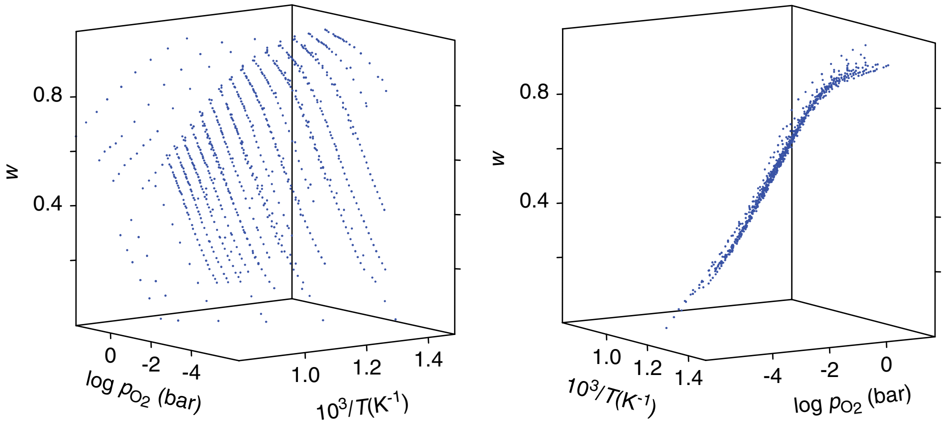

Fig. 16. Three-dimensional overall plot of the raw data used in Fig. 15.

metry range is covered by data. The rotated plot on the right-hand side gives a look at the data from the direction of the p_{O_2}, T dependences for constant composition; ideally along straight lines (Fig. 12) giving a sharp S-type profile.

In Table 6, the fitted thermodynamic parameters for the defect reactions of Table 5 are listed. The nonstoichiometry w and the defect concentrations calculated from these data are plotted in Fig. 17, where they are compared with isothermal data measured by Schleger et al. [21]. We see that both the point of integer valence, $[e'] = [h^\bullet]$, on the left-hand side and the point of the integer structure, $[\mathrm{O}_i''] = [v_\mathrm{O}^{\bullet\bullet}]$, on the right-hand side of the plot move toward higher partial pressures of oxygen with increasing temperature. This corresponds to the chemically reducing (deoxidizing) effect of temperature for oxides. Increasing temperature also increases concentrations of Frenkel defects, because the process of their formation has positive entropy. With $\Delta S^\circ_\mathrm{i}$ and $\Delta S^\circ_\mathrm{ox}$ being zero, the same positive value refers to the entropy of reduction, in agreement with formation of the O_2 gas under this process.

Table 6
Thermodynamic parameters of defect reactions obtained by fitting

Process	ΔS° ($\mathrm{J\,mol^{-1}\,K^{-1}}$)	ΔH° ($\mathrm{kJ\,mol^{-1}}$)
Frenkel	70.0 ± 0.4	112.7 ± 1.2
Ionization	0	34.1 ± 1.0
Oxidation	0	32.7 ± 1.3
Reduction	$\Delta S^\circ_\mathrm{F} + 2\Delta S^\circ_\mathrm{i} – \Delta S^\circ_\mathrm{ox} = 70.0$	$\Delta H^\circ_\mathrm{F} + 2\Delta H^\circ_\mathrm{i} – \Delta H^\circ_\mathrm{ox} = 148.2$

The pressure standard state is 1 bar O_2

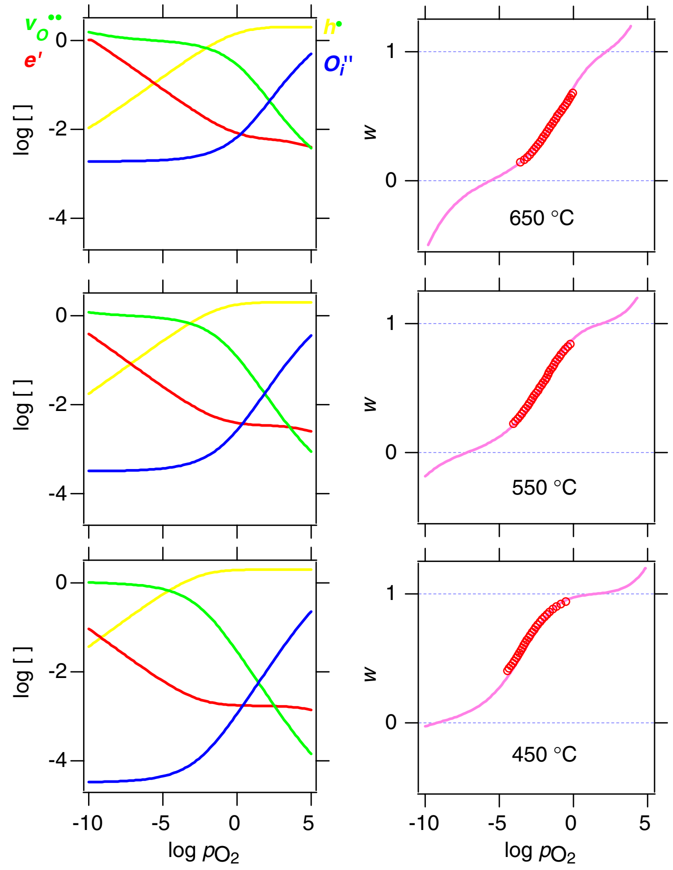

Fig. 17. Calculated defect concentrations and w in $YBa_2Cu_3O_{6+w}$ for temperatures corresponding to data by Schleger et al. [21] marked with circles.

Because e' and O_i'' are minority defects throughout the experimental data span, verification of their concentrations would require expanding the experimental data. In particular, pure electronic conductivity and equilibrium data for the superoxidized state with $w > 1$ would be needed.

3.5. Further simplifications?

When the Frenkel reaction in Table 5 is subtracted from the oxidation reaction, a pseudochemical reaction for oxidation of the oxygen vacancies is obtained:

$$\tfrac{1}{2}\mathrm{O}_{2(g)} + v_\mathrm{O}^{\bullet\bullet} = O_\mathrm{O}^{\times} + 2h^\bullet. \tag{2}$$

The same procedure done with enthalpies in Table 6 yields $\Delta H^\circ = -80\,\mathrm{kJ\,mol^{-1}}$; a value close to $\Delta H^\circ = –83\,\mathrm{kJ\,mol^{-1}}$ obtained by Mehta and Smyth [20] by using Eq. (2) to fit the nonstoichiometry data of Lindemer et al. [23]. The mass-action term for Eq. (2) is $K_\mathrm{vox} = p\mathrm{O}_2^{-1/2} 4w^2/(1-w)$, considering $[h^\bullet] \approx 2w$ and $1–[v_\mathrm{O}^{\bullet\bullet}] \approx w$. The quadratic equation has a straightforward solution for w as a function of p_{O_2}. Because this approach neglects the minority defects e' and O_i'', its validity range is limited. However, in the interval $0.3 < w < 1$, it gives practically the same fit as the full defect model shown in Fig. 15. In Ref. [20] also $[O_\mathrm{O}^{\times}] = 6 + w$ is included in the mass-action term of Eq. (2), leading to a marginal improvement of the fit with the resulting cubic algebraic equation.

3.6. Other oxides

The doping model presented for $YBa_2Cu_3O_{6+w}$ may be applicable to other oxides where the wide nonstoichiometry is accommodated in predominantly random manner. Modifications of such models would concern the type of the point defects present, but also the matter of coincidence of the integer structure with the integer valence. The integer (stoichiometric) valence state does not have to occur at an integer structure situation, yet doping still may be applicable to define the integer structure at which the nonstoichiometry range begins or ends. For that matter, that particular integer structure does not have to be thermodynamically stable. Neither has the doping to be real; the direction and width of the nonstoichiometry interval in electron units can be put directly into the electroneutrality condition that balances the defect charges. In such cases, a phenomenological description of the oxygen content as a function of the equilibrium partial pressure of oxygen is obtained. It is the latter dependence, which is the starting point for the oxygen-content control in the oxide as the first step to control its properties.

4. Oxygen-content control

Several methods how to control the oxygen nonstoichiometry in transition metal oxides have been invented, and reinvented. There is a common denominator to all of them: equilibrium. This equilibrium stems from point-defect considerations and concerns the oxygen exchange between the sample and the surrounding gas atmosphere. Typically, elevated temperatures need to be adopted for this equilibrium to be established in reasonable time. There is no simple rule for what this time needs to be for various oxides, but some guidance can be drawn from the following facts: the oxygen-exchange reaction is composed of two processes. The first is the surface reaction where O_2 splits into two oxygen anions and two holes or vice versa. This is the actual chemical oxidation (or reduction when in the opposite direction), because the holes represent the oxidized specie of the transition metal. The subsequent process is a diffusion-driven homogenization during which the surface oxygen excess (or its lack) homogeneously extends across the bulk of the sample. Because this happens via transport of oxygen ions and holes, high concentrations of electronic and structural defects (vacancies) are helpful. Such an oxide is a good electronic–ionic (or, shortly, mixed) conductor. Typically, the diffusion process has an activation energy, and, below some 200 °C, the equilibrium times for compact bulk samples of several millimeters size become several months even for best mixed conductors.

There are several control parameters that may be used to maintain the high-temperature equilibria and establish the desirable oxygen content in the sample. These parameters are listed in Table 7. Given that sufficient time is allowed for equilibration, two parameters must be maintained in open systems whereas in closed systems only one. The critical question is the regime of the cooling down.

4.1. Open systems of nonstoichiometry control

Open systems allow for flowing reaction atmospheres. The gas carries away products of decomposition of eventual gas-forming impurities such as carbonates, hydroxides, nitrates, etc. As a result, high purity of the oxide is maintained. In process 1 of Table 7, the sample is warmed to the temperature T while p_{O_2} in the flowing gas atmosphere is controlled. Oxygen partial pressures in the interval $10^{-5} < p_{O_2} < 10^{0}$ bars can be achieved by mixing of $O_{2(g)}$ and $Ar_{(g)}$, eventually also $H_2O_{(g)}$, and these pressures do not depend on temperature. Low partial pressures of oxygen can be controlled by mixing $H_{2(g)}$, $Ar_{(g)}$ and $H_2O_{(g)}$, and these do depend on temperature. This is because p_{O_2} is controlled not by the direct O_2 input, as in the $O_{2(g)}$–$Ar_{(g)}$ mixtures, but by the equilibrium $H_{2(g)} + ½O_{2(g)} = H_2O_{(g)}$, which is established with good kinetics above some 550 °C, depending somewhat on the catalytic ability of the sample. A practical upper limit for p_{O_2} occurs at about 10^{-10} bar, when the hydrogen dilution by argon approaches the level of $O_{2(g)}$ as an impurity or a leak gas. This means that for intermediate partial pressures of oxygen, between 10^{-5} and 10^{-10} bar, mixtures CO–CO_2 or CO_2–H_2 must be adopted. These mixtures are known for sluggish equilibrium in the gas phase, which consequently depends on catalysis effect of the sample [24].

Table 7
Parameters of nonstoichiometry control in oxides

Process	Control parameters	Red–ox reagent	System
1	p_{O_2}, T	Flowing gas of defined p_{O_2}	Open
2	Mass, T	Flowing gas of fixed p_{O_2}	Open
3	T	p_{O_2} buffer	Closed
4	Mass	Oxygen getter or source	Closed

The chemist should be aware of possible detrimental reactions in the just described atmospheres: Hydrogen is able to protonize oxide ions to form hydroxide defects upon corresponding reduction, while H_2O would protonate without reduction under formation of two hydroxide groups. Carbon dioxide may form carbonates with the most electropositive metals of the oxide. Both the protonation and carbonation will be suppressed by adopting a suitably high temperature for the nonstoichiometry control. However, at such temperatures, other forms of sample degradation are a problem. Apart from trivial cases of the complete reduction of the oxide into the metal, "evaporation" of lower oxides in reducing atmospheres is possible via gas-phase transport of the metal of favorably high partial pressure. This happens to manganese oxides in hydrogen atmospheres above some 1000 °C. Also, the carbon-based gas mixtures carry similar caveats, as carbide-oxides may in part be formed at very high temperatures for several early transition metals with strong affinity to both oxygen and carbon; say, up to Mn.

In modification 2 of the open process in Table 7, the sample is warmed in a thermobalance in a flow of gas with fixed p_{O_2} to such a temperature T that results in the loss or gain in mass expected to achieve the desirable oxygen nonstoichiometry. Use of time as a variable to control the oxygen content in a thermobalance is not advisable because highly inhomogeneous samples are obtained, out of equilibrium.

Clearly, samples that are equilibrated in the open systems must be quenched, because otherwise they would oxidize during the cool down. There are several experimental solutions to such quenching, and these are sketched in Fig. 18. Note that most of commercial thermobalances do not allow quenching the samples, but some of them may allow lowering the sample into a cooler region.

4.2. Closed systems of the nonstoichiometry control

For process 3 and 4 of Table 7, sealed-ampoule techniques are adopted. One of the consequences is that all impurities remain in the system, and the only possibility

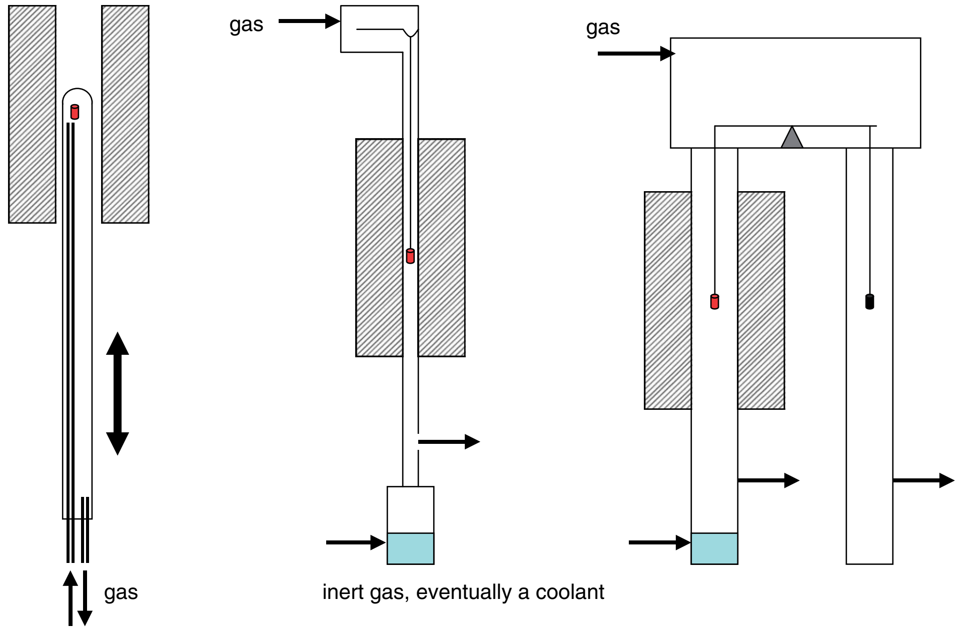

Fig. 18. Quenching from open systems of nonstoichiometry control.

to further purify the oxide is to add a substance that will absorb a specific impurity, for example, BaO_2 for CO_2 in oxygen-rich environments.

The oxygen-pressure buffer technique (number 3 in Table 7) utilizes the fact that the oxygen partial pressure is constant above a mixture of a metal and its compositionally adjacent oxide, or of two such metal oxides. The buffer must be in excess; so long it consists of both phases, the only parameter to control is temperature. Several such buffers have been used, as an example, Ni–NiO, Cu–Cu_2O, Cu_2O–CuO in Ref. [25], Fe–$Fe_{1-x}O$ in Ref. [26]. Partial pressures of oxygen for the copper-based buffers are plotted in Fig. 19.

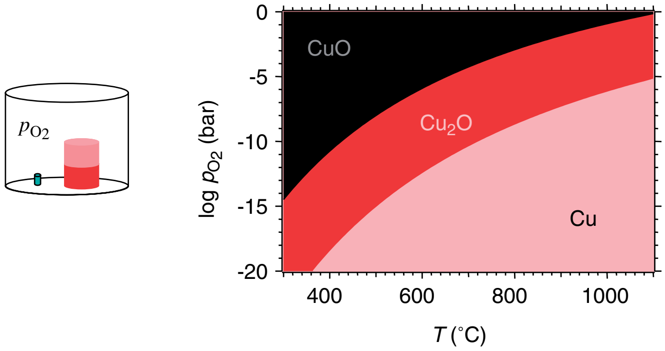

Fig. 19. Ranges of the copper-based p_{O_2} buffers.

A modification of the buffer technique for high pressures of O_2 utilizes substances that have high decomposition pressures of oxygen at the chosen oxygen-saturation temperature for the oxide sample. Such a substance is added in excess into the closed system with the oxide. For very high pressures, CaO_2, SrO_2 [27] and Ag_2O_2 [28] have been used; in this case not in ampoules, but rather in autoclaves or anvil cells. Solid XeO_3 would be a good oxidizing substance yielding exclusively inert products, but its tendency to self-accelerating decompositions makes it unsafe. Although introducing other chemical elements may pose risk for the purity of the oxide product, $KClO_3$ and $KClO_4$ have been popular for high-pressure syntheses and oxidations in anvil-cell and belt-type presses [29,30].

The oxygen-getter/oxygen-source techniques of process 4 of Table 7 are similar, but here it is the *amount* of the added substance that controls the oxygen content change. Either an amount of oxygen is taken by the getter, or released by the source. Although the mass is the controlling parameter, attention must be paid to the generated partial pressure of oxygen as well, so that the getter is thermodynamically able to reduce the oxide. The most commonly used getter is zirconium metal, which completely and rapidly oxidizes into ZrO_2. This is because the oxide is a very good oxygen-ion conductor and does not prevent access of oxygen to the metal. At 700 °C, a Zr foil 0.1 mm thick is completely oxidized within 2–3 weeks in a getter application. Advantages are the high substance purity of the foil and the stoichiometrically well-defined product ZrO_2, which, moreover, is rather inert toward quartz. The disadvantage of Zr is that only strongly oxidizing oxides can be reduced in this manner. Already an Fe(III) to Fe(II) reduction is beyond the ability of this getter. For such reductions, rare-earth metals, zinc or magnesium powder must be employed, the latter in such a thermal regime that MgO is formed quickly, protecting the quartz ampoule which otherwise is rapidly reduced itself. Zinc needs to be put into a corundum container, because ZnO reacts easily with SiO_2. When not reduction but oxidation is the goal, oxygen sources of well-defined composition and inert products are used to weigh in the needed amount of oxygen. As an example, Ag_2O in quartz ampoules is suitable for up to about ambient O_2 pressures above some 450 °C but below the melting point of Ag, above which the melt would dissolve some O_2 [31].

A very versatile and widely used modification of the getter/source technique is the solid-state coulometry, where the specified amount of oxygen is dosed to or from the enclosed sample electrochemically, via an oxide-ion conductor such as stabilized ZrO_2 [32].

5. Control of the nonstoichiometry distribution

Appropriate cooling regime is critical to all techniques of nonstoichiometry control. During cooling, high temperature gradients may be generated between the surface and the center of the sample, resulting in oxidation of the surface at the expense of the center. For best results, very rapid cooling should be adopted when the sample has access to oxygen; certainly in all open systems. Very slow cooling should be adopted for the low-p_{O_2} getter techniques where no O_2 is left to oxidize the sample. Efficient techniques for achieving high compositional and crystalline perfection have been developed, for example, by Brabers [33] for nonstoichiometry control in magnetite. However, even with all precautions, certain gradient of the oxygen content in the bulk of the oxide is inevitable. In particular, the open-system methods are prone to generating a distribution of oxygen contents in the sample.

6. Evaluation of the nonstoichiometry distribution

The nonstoichiometry distribution may concern the bulk of the sample, but also the individual grains when the sample is porous. Particularly instructive are cases when the oxygen-content inhomogeneity can be evaluated visually, such as in contrast of the typically dark-colored nonstoichiometric area with the light-colored pure stoichiometric oxide. For quantitative evaluations, in cases of no color difference, or when inhomogeneity of individual grains is suspected, the distribution of the oxygen nonstoichiometry may be evaluated from profile analysis of a Bragg reflection in an X-ray powder diffraction pattern of the sample. This analysis requires prior knowledge of unit-cell parameters as functions of oxygen nonstoichiometry. The examined Bragg peak, of a tailed or broadened profile, is reconstructed from convolution of an array of Lorentzian peaks of instrument width across the profile's angular range. The unit-cell parameter's function of the nonstoichiometry links the Bragg angles of these component peaks to the nonstoichiometry level of the fraction of the phase defined by the component peak's intensity. This method is suitable for least-squares fitting. For increased validity of such results, Bragg peaks specific to each of the unit-cell parameters should be selected for the analysis, and strain and particle size effects should be evaluated in advance from Williamson–Hall plots. An example of such a result [34] is shown in Fig. 20.

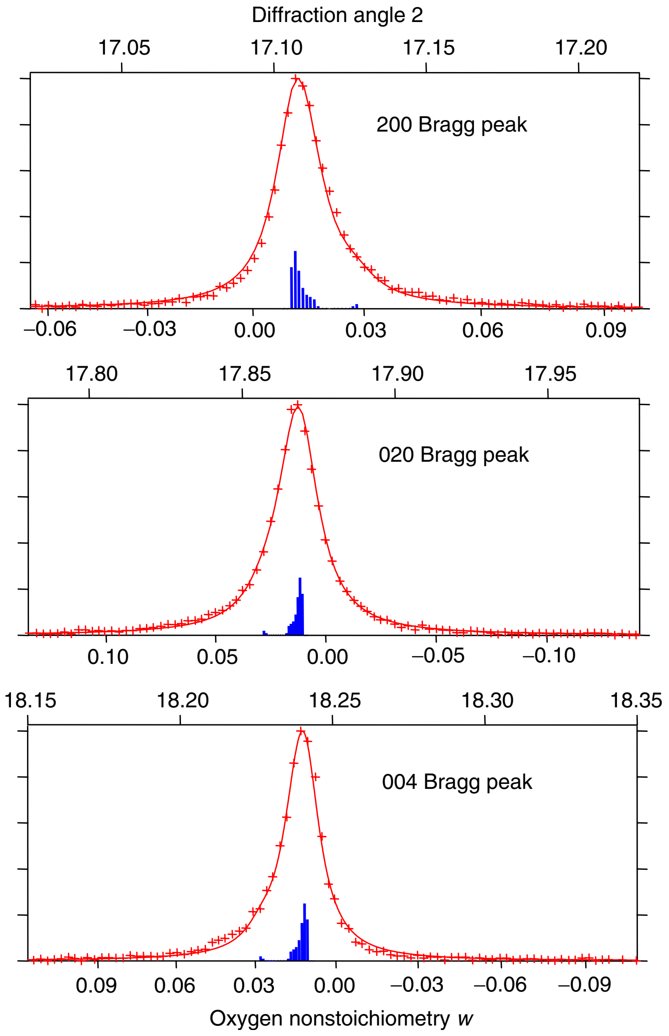

Fig. 20. Distribution of oxygen nonstoichiometry w in $GdBaFe_2O_{5+w}$ according to fitting Bragg profiles of the synchrotron X-ray powder diffraction pattern.

7. Analyses of bulk oxygen nonstoichiometry

In situ thermogravimetry is perhaps the most universal method of nonstoichiometry analysis. However, precise results worth the effort are obtained only with high-precision thermobalances under procedures that eliminate the instrument drift, prevent loss of volatile non-oxygen species, and pinpoint precisely the reference stoichiometric state. Consequently, high-precision thermogravimetry is most suited for devoted studies of oxygen nonstoichiometry rather than to obtain a single analysis result characterizing a bulk oxide. Such a quick analysis of sufficiently high precision is better obtained by wet (chemical) titration methods. Because moles rather than mass of oxygen are measured in this manner, wet titration methods are less sensitive to small levels of impurities in metal oxides. In fact, the simplest case of such titration analysis only requires that the sample has maintained the nominal stoichiometry of metallic elements (if there is several) as introduced by weighing at the beginning of the synthesis. This is a reasonable assumption when analyzed and standardized reagents of high substance purity are used and synthesis conditions adopted that prevent specific loss of a metallic element. One single titration is then needed for the nonstoichiometry analysis.

Iodometric and cerimetric red–ox titrations are suitable for determinations of significant[7] levels of nonstoichiometry in metal oxides. Note that any assignment of the result as an actual (and not only nominal) nonstoichiometry is contingent upon proof of the single-phase character and identity of the oxide by high-quality X-ray diffraction.

7.1. Iodometry

Iodometry is suitable for highly oxidizing oxides that quantitatively convert iodide to iodine (tri-iodide anion) in aqueous HCl solutions. Iodine is titrated by a thiosulfate solution of precise molarity in a very distinct titration, in which the color change is enhanced by addition of soluble starch right before the point of equivalence. The nonstoichiometry that is suitable for iodometric analysis occurs in two types of elements: (1) those in highly oxidizing valence states that reduce to stable non-oxidizing ions in aqueous solutions, (2) those in valences that reduce into states stabilized by formation of an iodide complex, soluble or insoluble. The first type includes any[8] nonstoichiometry *above the following oxidation states*: trivalent Cr [35], divalent Mn [36], divalent Co [36], divalent Ni [37], trivalent Ce, trivalent Tb, and trivalent Pr. Also, pentavalent vanadium oxidizes iodide quantitatively [38], suggesting that nonstoichiometry above tetravalent V could possibly be analyzed iodometrically. An example of the second type is determination of any nonstoichiometry above monovalent Cu [39]. Nonstoichiometry of oxides containing several such elements is also determined in one titration: Co,Cu [40], Co,Mn [41], Cu,Tb [42], Cu,Pr [42]. However, iodometric analyses in combination with any iron species require cautions because iodide is oxidized only incompletely by trivalent iron. Complexing may be used to decrease the standard potential of trivalent iron so that the oxidation is suppressed and iodometric analysis can be performed exclusively on the suitable element, such as Co [43]. Alternatively, cerimetric analysis is more versatile for similar nonstoichiometry determination [44].

7.2. Cerimetry

Cerimetry utilizes an Fe(II) 1,10-phenanthroline complex (Ferroin), which is reversibly discolored in its oxidized form upon titration with a Ce^{4+} solution. Being thus linked to the Fe^{3+}/Fe^{2+} red–ox pair, cerimetry can be used for analyses of nonstoichiometry levels that either oxidize Fe^{2+} or reduce Fe^{3+}. For the case of oxidation, a precise excess of high-purity crystalline Mohr's salt is added upon the oxide digestion in aqueous HCl, for the case of reduction, an excess of 1 M $FeCl_3$ is added. Subsequently, Fe(II) is titrated. Because the Ce^{4+} solution is prone to hydrolysis, the titration is done in a strongly HCl-acidic solution into which some H_3PO_4 was added to obtain a less colored phosphatocomplex of Fe(III). In such mixtures, the standard potential E° for tri-/divalent iron is 0.6 V [45]; well positioned for quantitative reaction with many red–ox systems of metallic elements.

According to tabulated values of standard potentials at $pH = 0$ for the first-row transition elements, any nonstoichiometry *below the following oxidation states* will reduce 1 M $FeCl_3$ solution whereas any nonstoichiometry *above them* will oxidize the Mohr's salt: tetravalent Ti, tetravalent V, trivalent Cr, divalent Mn, divalent Co, divalent Ni. In addition, any nonstoichiometry in the Fe^{III}–Fe^{II} range is titrated directly with no additives [31], any nonstoichiometry below divalent iron will reduce 1 M $FeCl_3$ whereas any nonstoichiometry above trivalent iron will oxidize Mohr's salt [31]. In the second- and third-row transition metals, only the early elements would be suitable for the titration, and the limiting oxidation states are: tetravalent Zr, pentavalent Nb, tetravalent Mo, tetravalent Hf, pentavalent Ta, hexavalent W. Standard potentials involving rhenium ions are too close to E° for Fe^{3+}/Fe^{2+} as well as to each other, and similar unfavorable situation occurs for practically all light and heavy platinum metals, with few exceptions. The alternative analysis for these metals is the reduction to metal in a gravimetric setup. Nonstoichiometry of oxides containing several elements in oxidation states suitable for cerimetry is determined in one titration, as an example, the V, Mo combination [46].

In some cases, the titration method allows determining the average oxidation number of a metal independent of other metals in the oxide. Two titrations are then required, one for the nonstoichiometry and one that determines the content of the concerned metal. Chemistry of copper is favorable for such analyses. Any nonstoichiometry above divalent copper is analyzed by two straightforward iodometric titrations [12]. Analysis of any nonstoichiometry above monovalent copper requires an intermittent oxidation by H_2O_2 prior to quantitative reduction by HCl to Cu^{2+} for analysis of total Cu. Also iron allows applying two cerimetric titrations, the second involving quantitative reduction with $SnCl_2$ to Fe^{2+} prior titration of the total iron; for analyses of any nonstoichiometry above divalent iron [31].

---

[7] Above what corresponds to some 0.004 valence units of the metal atom concerned. Standard deviations better than 0.002 valence units, typically 0.001; for manual titrations with standard 10 mL burette.

[8] For the following elements, it includes all their higher oxidation states; something that not always is the case.

7.3. Digestion of the solid oxide

The key technique that makes the above titrations simple and applicable to analyses of nonstoichiometry in various solid oxides is closed-ampoule digestion [47]. Given sufficient time, many finely pulverized nonstoichiometric oxides will dissolve in hydrochloric acid or otherwise react with the red–ox additive when heated in a sealed glass ampoule. Even rather inert oxides such as $LaCrO_3$ react within hours at 100 °C [48]. Most oxides take only a minute or so [49]. The dissolutions can be enhanced by ultrasound agitation [50]. For careful work, a blank procedure should be performed (dissolution and titration without presence of the sample), in particular for iodometry where a small concentration of iodine may be generated by thermal splitting of HI. A quantitative example on the ampoule technique of oxide digestion is given in Ref. [41].

Cautionary note: dissolutions accompanied by evolution of gas can explode the glass ampoule and cause harm. Attention needs to be paid to the presence of oxycarbonates or residual carbonates in the samples, which may go undetected or unsuspected, but is manifested by rapid evolution of CO_2 in the acid solution. Evolution of hydrogen due to the eventual presence of electropositive elementary metals in the samples proceeds usually slower.

8. In conclusion

Tailoring oxide materials to desired properties typically requires good control over oxygen nonstoichiometry. In cases of strongly correlated properties that are linked to precise valence states, such as spin-state transitions, orbital ordering transitions and hole–electron singularities, the control of the oxygen content distribution across the sample is essential. A typical example of such an oxide is magnetite, a half-metallic oxide suitable as a source of spin-polarized electrons for spintronic devices. The property control in the case of Fe_3O_4 goes even beyond the simple homogeneity of the oxygen content and into questions of the single-crystalline perfection itself [51].

References

[1] W.G. Burns, T.F. Williams, Nature (London) 175 (1955) 1043–1044.
[2] A.T. Collins, Diam. Relat. Mater. 12 (2003) 1976–1983.
[3] D.C. Hunt, D.J. Twitchen, M.E. Newton, J.M. Baker, T.R. Anthony, W.F. Banholzer, S.S. Vagarali, Phys. Rev. B: Condens. Matter 61 (2000) 3863–3876.
[4] J.S. Anderson, J. Chem. Soc. Dalton Trans. Inorg. Chem. (1973) 1107–1115.
[5] F.A. Kröger, H.J. Vink, Solid State Phys. 3 (1956) 307–435.
[6] P. Kofstad, Non-stoichiometry, Diffusion and Electrical Conductivity in Binary Metal Oxides, Wiley, New York, 1972.
[7] D.M. Smyth, The Defect Chemistry of Metal Oxides, Oxford University Press, Oxford, 2000.
[8] M.M. El-Aiat, F.A. Kröger, J. Am. Ceram. Soc. 65 (1982) 162–166.
[9] A. Holt, P. Kofstad, Solid State Ionics 69 (1994) 127–136.
[10] A. Holt, P. Kofstad, Solid State Ionics 100 (1997) 201–209.
[11] J.S. Anderson, Surf. Defect Prop. Solids 1 (1972) 1–53.
[12] H. Fjellvåg, P. Karen, A. Kjekshus, P. Kofstad, T. Norby, Acta Chem. Scand. Ser. A 42 (1988) 178–184.
[13] J. Maier, H.L. Tuller, Phys. Rev. B: Condens. Matter 47 (1993) 8105–8110.
[14] P. Meuffels, R. Naeven, H. Wenzl, Physica C (Amsterdam) 161 (1989) 539–548.
[15] T. Mathews, K.T. Jacob, Metall. Trans. A: Phys. Metall. Mater. Sci. 23A (1992) 3325–3335.
[16] G.F. Voronin, Pure Appl. Chem. 72 (2000) 463–477.
[17] P. Karen, A. Kjekshus, Phase diagrams and thermodynamic properties, Handbook on the Physics and Chemistry of Rare Earths, vol. 30, 2000, pp. 229–373.
[18] E.K. Chang, D.J.L. Hong, A. Mehta, D.M. Smyth, Mater. Lett. 6 (1988) 251–253.
[19] K. Kishio, K. Suzuki, T. Hasegawa, T. Yamamoto, K. Kitazawa, K. Fueki, J. Solid State Chem. 82 (1989) 192–202.
[20] A. Mehta, D.M. Smyth, Phys. Rev. B: Condens. Matter 51 (1995) 15382–15387.
[21] P. Schleger, W.N. Hardy, B.X. Yang, Physica C (Amsterdam) 176 (1991) 261–273.
[22] K. Conder, J. Karpinski, E. Kaldis, S. Rusiecki, E. Jilek, Physica C (Amsterdam) 196 (1992) 164–170.
[23] T.B. Lindemer, J.F. Hunley, J.E. Gates, A.L. Sutton Jr., J. Brynestad, C.R. Hubbard, P.K. Gallagher, J. Am. Ceram. Soc. 72 (1989) 1775–1788.
[24] A. Benisek, W. Sitte, J. Electrochem. Soc. 152 (2005) H157–H160.
[25] P. Karen, O. Braaten, H. Fjellvåg, A. Kjekshus, Compatibilities of $YBa_2Cu_3O_{9-\delta}$ type phase in quintenary systems yttrium–barium–copper–oxygen–X (impurity), NASA Conference Publication, 1991, 3100 (AMSAHTS '90: Adv. Mater. Sci. Appl. High Temp. Supercond.), pp. 117–126.
[26] J. Nakamura, J. Linden, H. Suematsu, M. Karppinen, H. Yamauchi, Physica C (Amsterdam) 338 (2000) 121–125.
[27] M. Ushiki, T. Motohashi, H. Yamauchi, M. Karppinen, Physica C (Amsterdam) 378–381 (Part 1) (2002) 167–172.
[28] M. Karppinen, H. Yamauchi, Y. Morita, M. Kitabatake, T. Motohashi, R.S. Liu, J.M. Lee, J.M. Chen, J. Solid State Chem. 177 (2004) 1037–1043.
[29] G. Demazeau, B. Buffat, M. Pouchard, P. Hagenmuller, Z. Anorg. Allg. Chem. 491 (1982) 60–66.
[30] M. Karppinen, H. Yamauchi, H. Suematsu, O. Fukunaga, Physica C (Amsterdam) 264 (1996) 268–274.
[31] P. Karen, A. Kjekshus, J. Solid State Chem. 112 (1994) 73–77.
[32] B.C.H. Steele, Nat. Bur. Stand. (US) Spec. Publ. (296) (1968) 165–172.
[33] V.A.M. Brabers, F. Walz, H. Kronmüller, Phys. Rev. B: Condens. Matter 58 (1998) 14163–14166.
[34] P. Karen, J. Solid State Chem. 170 (2003) 9–23.
[35] S.W. Weller, S.E. Voltz, J. Am. Chem. Soc. 76 (1954) 4695–4701.
[36] H.B. Sachse, Anal. Chem. 32 (1960) 529–530.
[37] J. Dereń, J. Haber, J. Słoczyński, Chem. Anal. (Warsaw) 6 (1961) 659–662.
[38] B. Kirson, M. Bobtelsky, Bull. Soc. Chim. France (1947) 560–563.
[39] A. Manthiram, J.S. Swinnea, Z.T. Sui, H. Steinfink, J.B. Goodenough, J. Am. Chem. Soc. 109 (1987) 6667–6669.
[40] Q. Huang, P. Karen, V.L. Karen, A. Kjekshus, J.W. Lynn, A.D. Mighell, I.N. Sora, N. Rosov, A. Santoro, J. Solid State Chem. 108 (1994) 80–86.
[41] P. Karen, E. Suard, F. Fauth, P.M. Woodward, Solid State Sci. 6 (2004) 1195–1204.
[42] P. Karen, H. Fjellvåg, O. Braaten, A. Kjekshus, H. Bratsberg, Acta Chem. Scand. 44 (1990) 994–1001.
[43] P.H. Andresen, H. Fjellvåg, P. Karen, A. Kjekshus, Acta Chem. Scand. 45 (1991) 698–708.
[44] Q.Z. Huang, V.L. Karen, A. Santoro, A. Kjekshus, J. Linden, T. Pietari, P. Karen, J. Solid State Chem. 172 (2003) 73–80.
[45] D.A. Skoog, D.M. West, Fundamentals of Analytical Chemistry, fourth ed., 1982, p. 324.

[46] P. Karen, A.R. Moodenbaugh, J. Goldberger, P.N. Santhosh, P.M. Woodward, J. Solid State Chem. 179 (2006) 2120–2125.

[47] I.N. Sora, Q. Huang, J.W. Lynn, N. Rosov, P. Karen, A. Kjekshus, V.L. Karen, A.D. Mighell, A. Santoro, Phys. Rev. B: Condens. Matter 49 (1994) 3465–3472.

[48] P. Karen, T. Norby, J. Electrochem. Soc. 145 (1998) 264–269.

[49] P. Karen, P.M. Woodward, J. Solid State Chem. 141 (1998) 78–88.

[50] P. Karen, H. Fjellvåg, A. Kjekshus, A.F. Andresen, J. Solid State Chem. 92 (1991) 57–67.

[51] F. Walz, V.A.M. Brabers, H. Kronmüller, J. Phys. IV C 1 (1997) 569–572.